Photocatalysis
Research and Potential

SCIEPublish

Article

Sustainable Silver Recovery from End-of-Life Photovoltaic Panels and Photocatalytic Valorization

Xinru Wang [1], Yao Chen [1,*], Xinwei Wang [1], Zhenyu Wang [1], Yuchen Zhang [1], Hisao Yoshida [2], Hiromi Yamashita [1,3,4,*] and Zhenfeng Bian [1,*]

[1] MOE Key Laboratory of Resource Chemistry and Shanghai Key Laboratory of Rare Earth Functional Materials, Shanghai Normal University, Shanghai 200234, China; 212201307@shnu.edu.cn (X.W.); 230113879@shnu.edu.cn (X.W.); 230113880@shnu.edu.cn (Z.W.); 250143926@shnu.edu.cn (Y.Z.)

[2] Graduate School of Human and Environmental Studies, Kyoto University, Yoshida Nihonmatsu-cho, Sakyo-ku, Kyoto 606-8501, Japan; yoshida.hisao.2a@kyoto-u.ac.jp (H.Y.)

[3] SANKEN, The University of Osaka, 8-1 Mihogaoka, Ibaraki, Osaka 567-0047, Japan

[4] Division of Materials and Manufacturing Science, Graduate School of Engineering, The University of Osaka, 2-1 Yamada-oka, Suita, Osaka 565-0871, Japan

* Corresponding author. E-mail: chenyao@shnu.edu.cn (Y.C.); yamashita@mat.eng.osaka-u.ac.jp (H.Y.); bianzhenfeng@shnu.edu.cn (Z.B.)

Received: 14 September 2026; Revised: 8 October 2026; Accepted: 30 October 2026; Available online: 13 November 2026

ABSTRACT: The rapid accumulation of end-of-life photovoltaic (PV) modules calls for the sustainable recovery of valuable metals contained within them. In crystalline silicon PV modules, silver (Ag) is the metal with the highest economic value, but its selective recovery remains challenging. Here, we report a method based on an ammonium molybdate tetrahydrate ($(NH_4)_6Mo_7O_{24}\cdot 4H_2O$)-hydrogen peroxide ($H_2O_2$) system for selectively leaching Ag from end-of-life PV modules. During the Ag recovery process, aluminum remains largely insoluble, while lead is partially leached and separated. During leaching, Ag^+ reacts *in situ* with molybdate ions to form silver molybdate ($Ag_xMo_yO_z$). Singlet oxygen ($^1O_2$), hydroxyl radicals (•OH), and peroxy (•OOH) radicals were identified as active species during the leaching process. The recovered silver molybdate can be directly used as a photocatalyst for pollutant degradation, providing proof of concept for a "waste-to-useful" strategy. This study establishes a closed-loop pathway from end-of-life PV modules to functional photocatalysts, eliminating the need for additional silver purification or catalyst synthesis steps.

Keywords: End-of-life photovoltaic panels; Silver recovery; Silver molybdate; Photocatalysis; Pollutant degradation

1. Introduction

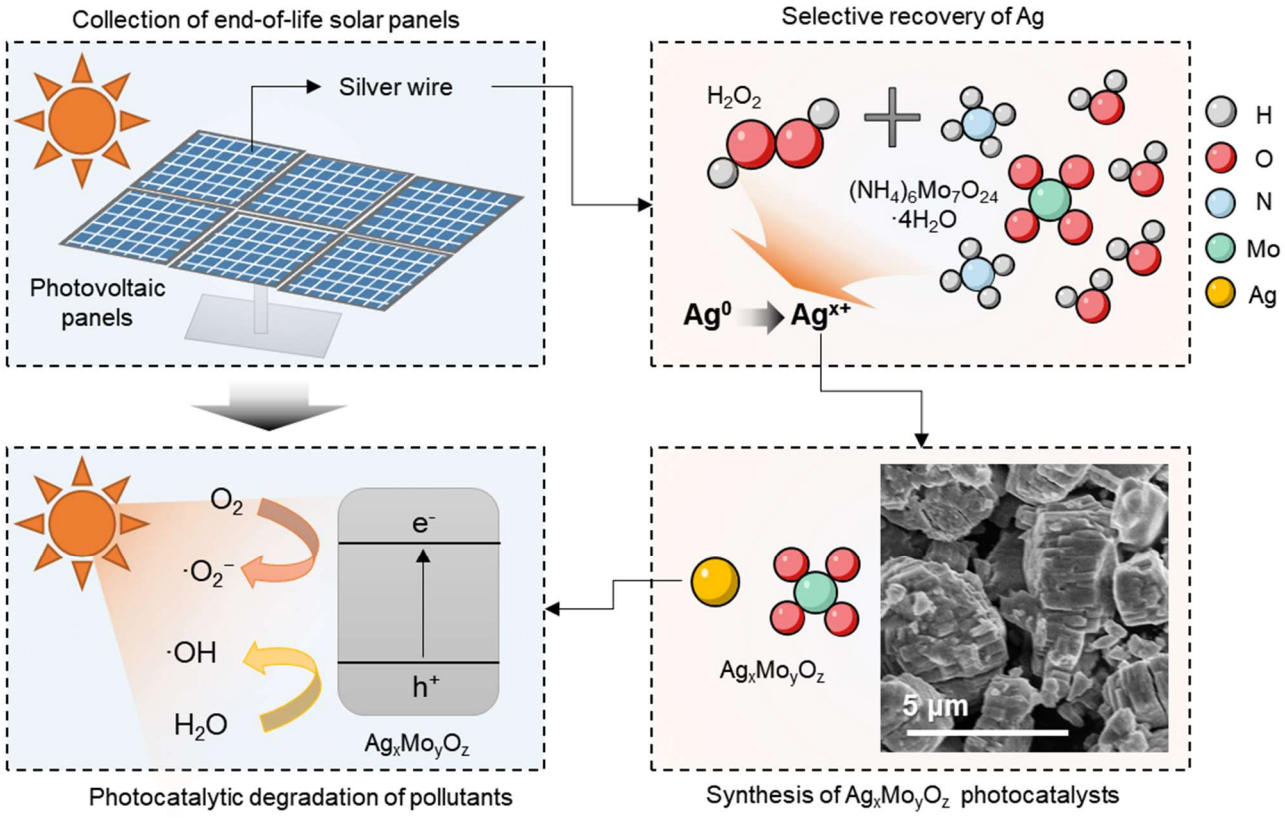
The rapid expansion of photovoltaic (PV) deployment has created a pressing waste management challenge [1,2]. Global end-of-life PV waste is projected to reach approximately 8 million tonnes by 2030 and nearly 78 million tonnes by 2050 [3,4]. Silver (Ag) is the most economically valuable metal in

© 2026 The authors. This is an open access article under the Creative Commons Attribution 4.0 International License (https://creativecommons.org/licenses/by/4.0/).

crystalline silicon PV modules, yet it accounts for only about 0.05% of the module mass [5,6]. Current recycling practices primarily target glass, Ag, silicon (Si), and aluminum (Al), while selective recycling technologies for Ag remain underdeveloped [7]. Effective Ag recovery is therefore important for both resource sustainability and environmental protection [8].

Ag recovery from PV panels mainly relies on hydrometallurgical leaching. Nitric acid (HNO_3) leaching achieves high Ag dissolution but generates nitrogen oxide (NO_x) emissions and co-dissolves Al [9,10]. Ammonia ($NH_3 \cdot H_2O$)-hydrogen peroxide (H_2O_2) systems avoid NO_x emissions by forming soluble silver-ammonia complexes [11]. However, $NH_3 \cdot H_2O$ volatilization creates operational and environmental concerns. Deep eutectic solvent (DES) systems have recently shown promising leaching performance, but their high viscosity and complex regeneration limit practical application [12,13]. Photocatalytic dissolution technology offers a mild leaching approach for precious metals, enabling the recovery of Ag, gold, and platinum group metals [14–16]. In addition, a common limitation of these methods is that the leaching step only produces an Ag-bearing solution. Additional purification or reduction steps are then needed to obtain a usable Ag product. This increases process complexity and reagent consumption.

This work explores a different route (Scheme 1). Ammonium molybdate tetrahydrate ($(NH_4)_6Mo_7O_{24} \cdot 4H_2O$) and H_2O_2 are used to leach Ag selectively from retired PV panels. Al remains essentially undissolved. The leached Ag is not kept in solution. Instead, it reacts in situ with molybdate to form silver molybdate ($Ag_xMo_yO_z$). This solid product is collected and used directly as a photocatalyst for pollutant degradation. Lead (Pb) is partially leached and separated during product recovery. The leaching process is driven by singlet oxygen ($^1O_2$), hydroxyl radicals (•OH), and peroxy (•OOH) radicals. The recovered $Ag_xMo_yO_z$ exhibits photocatalytic activity. This work demonstrates a closed-loop concept of treating waste with waste. It converts retired PV panels into functional photocatalysts without additional Ag purification or catalyst synthesis.



Scheme 1. Schematic diagram of a closed-loop strategy for the recovery of silver from end-of-life photovoltaic panels.

2. Materials and Methods

2.1. Chemicals and Materials

Ammonium molybdate tetrahydrate ($(NH_4)_6Mo_7O_{24}\cdot 4H_2O$, AR), ammonium molybdate anhydrous ($(NH_4)_2MoO_4$, AR), sodium molybdate (Na_2MoO_4, AR), ammonium iodide (NH_4I, AR), hydrogen peroxide (H_2O_2, 30 wt%, AR), Ethanol (C_2H_5OH, AR), methylene blue (MB), rhodamine B (RhB), furfuryl alcohol (FFA), isopropanol (IPA), 5,5-dimethyl-1-pyrroline N-oxide (DMPO), and 2,2,6,6-tetramethylpiperidine (TEMP) were purchased from Adamas-beta and used as received. Retired PV panels were procured from Alibaba. Deionized water was used throughout all experiments.

2.2. Pretreatment of End-of-Life Photovoltaic Panels

End-of-life crystalline silicon photovoltaic (PV) panels were collected and manually dismantled to obtain the silicon solar cells. The cells were cut into small pieces and cleaned with ethanol and deionized water to remove surface contamination.

2.3. Silver Leaching Experiments

Leaching experiments were carried out in a beaker under magnetic stirring. In a typical run, a piece of PV cell was immersed in a given volume of ammonium molybdate solution, and a predetermined amount of H_2O_2 was added to initiate the reaction. The effects of $(NH_4)_6Mo_7O_{24}\cdot 4H_2O$ concentration (5, 10, and 15 g/L), H_2O_2 concentration (0.5%, 1%, and 3%), temperature (20, 30, 40, 50, and 60 °C), and reagent addition mode were investigated. In the stepwise addition experiments, equal amounts of reagents were added in portions rather than all at once. To identify the roles of molybdate and ammonium, $(NH_4)_2MoO_4$, Na_2MoO_4, and NH_4I were used as alternative reagents. The leaching process was monitored by measuring the concentration of Ag, Al, Si, and Pb in the solution using inductively coupled plasma optical emission spectrometry (ICP-OES). Each experiment was performed in triplicate.

2.4. Recovery of Silver Molybdate

After leaching, the solid product was collected by rotary evaporation and filtration, washed repeatedly with deionized water and ethanol, and dried at 60 °C overnight. The obtained product was denoted as $Ag_xMo_yO_z$.

2.5. Photocatalytic Degradation Experiments

The photocatalytic activity of the recovered $Ag_xMo_yO_z$ was evaluated by degrading MB and RhB under visible light irradiation. In a typical experiment, 50 mg of catalyst was added to 20 mL of 10 ppm dye solution. The suspension was stirred in the dark for 30 min to reach adsorption-desorption equilibrium. Then, the suspension was irradiated with a visible light source. At given time intervals, aliquots were withdrawn and centrifuged to remove the catalyst. The dye concentration was measured by Ultraviolet-visible (UV-vis) spectrophotometry at the characteristic absorption wavelength. The degradation efficiency was calculated as $(C_0 - C_t)/C_0 \times 100\%$, where C_0 and C_t are the initial and time-dependent concentrations, respectively.

2.6. Radical Trapping and ESR Measurements

Radical trapping experiments were conducted to identify the active species in the leaching process. FFA and IPA were used as scavengers for $^1O_2$ and •OH, respectively. Electron spin resonance (ESR) spectroscopy was employed to detect reactive oxygen species using DMPO and TEMP as spin traps. ESR spectra were recorded at different reaction times to monitor the generation of $^1O_2$, •OH, and •OOH.

2.7. Characterization

The morphology and elemental distribution of the PV panels before and after leaching and the recovered product were examined by scanning electron microscopy (SEM) equipped with energy-dispersive X-ray spectroscopy (EDS). X-ray photoelectron spectroscopy (XPS) was used to analyze surface chemical states with a monochromatic Al Kα source. Fourier transform infrared (FTIR) spectra were recorded in the range of 400–4000 cm^{-1}. X-ray diffraction (XRD) patterns were collected on a powder diffractometer with Cu Kα radiation. UV-vis diffuse reflectance spectra (DRS) were obtained on a UV-vis spectrophotometer, and the band gap was calculated using the Tauc equation. The concentrations of metal ions in solution were determined by ICP-OES.

3. Results and Discussion

3.1. Selective Silver Leaching from End-of-Life Photovoltaic Panels

Ag leaching experiments were first conducted to evaluate the performance of the $(NH_4)_6Mo_7O_{24}\cdot4H_2O$-$H_2O_2$ system. The effect of $(NH_4)_6Mo_7O_{24}\cdot4H_2O$ concentration is shown in Figure 1a. At 5 g/L, Ag was completely leached within 120 min. Increasing the concentration to 10 or 15 g/L accelerated the leaching rate, with complete leaching achieved within 60 min. The effect of H_2O_2 concentration is shown in Figure 1b. At 0.5%, Ag leaching was incomplete. At 1%, complete leaching was achieved within 120 min. At 3%, the leaching time was further reduced to 60 min. The effect of reagent addition mode was also examined (Figure S1). Stepwise addition of $(NH_4)_6Mo_7O_{24}\cdot4H_2O$ showed no significant effect, whereas stepwise addition of H_2O_2 reduced the leaching rate to 20%. This is likely because H_2O_2 decomposes readily, and stepwise addition lowers its effective concentration during the reaction. Different molybdenum and ammonium sources were compared (Figure S2). Sodium molybdate (Na_2MoO_4) and ammonium iodide (NH_4I), which provide only molybdate or ammonium, respectively, showed no leaching ability. Anhydrous ammonium molybdate ($(NH_4)_2MoO_4$) achieved only 40% leaching. These results indicate that both molybdate and ammonium are essential for silver leaching, and the hydrated form of $(NH_4)_6Mo_7O_{24}\cdot4H_2O$ is important for optimal performance. The effect of temperature is shown in Figure 1c. The leaching rate increased with temperature up to 40 °C, at which complete leaching was achieved within 15 min. Further temperature increases slightly reduced the rate, possibly due to accelerated H_2O_2 decomposition.

The optimal conditions (3% H_2O_2 and 10 g/L $(NH_4)_6Mo_7O_{24}\cdot4H_2O$) were then applied to leach Ag from actual end-of-life PV panels. Figure 1d shows the scanning electron microscope (SEM) image and corresponding energy dispersive spectrometer (EDS) mapping of the pristine PV panel. Ag fingers were clearly visible, with high mapping contrast. Silicon (Si) was distributed alongside the Ag fingers, and Pb was located in the same regions as Ag [17]. After leaching, the Ag distribution was no longer evident, while the mapping signals of Si and Pb in the same regions became more pronounced (Figure 1e). Figure S3 shows the SEM and EDS mapping of the back side of the PV panel, where Al and Si were the main elements detected [18]. Little change was observed after leaching. The selectivity data are shown in Figure 1f. Ag was completely leached, while Al and Si were not leached at all. Pb showed partial leaching at 40%. This suggests that Pb is partially soluble under the leaching conditions, likely due to the formation of soluble Pb species, while aluminum trioxide (Al_2O_3) and silicon nitride (Si_3N_4) remain stable. X-ray photoelectron spectroscopy (XPS) was used to track chemical-state changes before and after leaching (Figure S4). Before leaching, Ag existed as both metallic Ag and silver oxide (AgO). After 30 min, metallic Ag was completely leached, leaving only AgO. After 1 h, all Ag species were removed from the PV panel. In contrast, Al, Pb, and Si remained as Al_2O_3, lead oxide (PbO), and Si_3N_4 throughout the process [19,20]. The PbO peak intensity decreased slightly after leaching, consistent with partial Pb leaching.

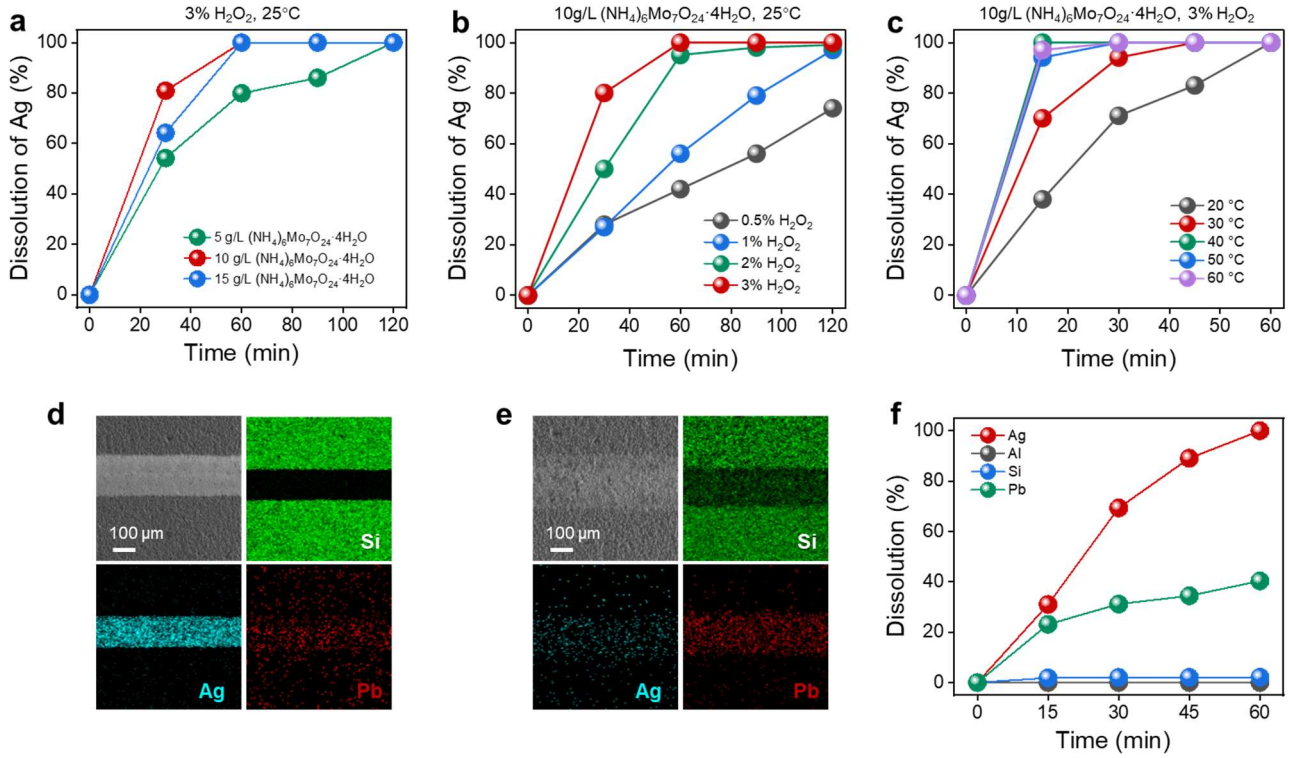


Figure 1. Silver leaching behavior from end-of-life photovoltaic panels. (**a**) Effect of $(NH_4)_6Mo_7O_{24}·4H_2O$ concentration on Ag leaching (3% H_2O_2, 25 °C). (**b**) Effect of H_2O_2 concentration on Ag leaching (10 g/L $(NH_4)_6Mo_7O_{24}·4H_2O$, 25 °C). (**c**) Effect of temperature on Ag leaching (10 g/L $(NH_4)_6Mo_7O_{24}·4H_2O$, 3% H_2O_2). (**d**) SEM image and corresponding EDS mapping of the pristine PV panel. (**e**) SEM image and corresponding EDS mapping of the PV panel after leaching. (**f**) Leaching selectivity of Ag, Al, Si, and Pb under optimized conditions.

3.2. Mechanistic Insights into Silver Leaching

To elucidate the leaching mechanism, the evolution of molybdenum species and reactive oxygen species (ROS) during the leaching process was systematically investigated. Liquid ultraviolet-visible (UV-vis) spectroscopy was first employed to monitor the reaction solution (Figure 2a). Upon addition of H_2O_2 to the $(NH_4)_6Mo_7O_{24}·4H_2O$ solution, a new absorption peak emerged at approximately 310 nm, which is characteristic of the diperoxo molybdate complex $MoO_2(O_2)_2^{2-}$ [21]. This observation confirms the formation of a Mo(VI)-peroxo intermediate. Raman spectroscopy provided further structural evidence for the peroxo species (Figure 2b). In the absence of H_2O_2, the $(NH_4)_6Mo_7O_{24}·4H_2O$ solution exhibited a strong band at 947 cm^{-1} along with shoulders at 899 and 947 cm^{-1}, indicating that the predominant Mo species is the heptamolybdate ion $Mo_7O_{24}^{6-}$. Upon addition of H_2O_2, new bands appeared at 540 and 872 cm^{-1}, which are assigned to the stretching vibrations of [$Mo(O_2)$] and [O–O] bonds, respectively [22]. The band at 971 cm^{-1} corresponds to the [Mo=O] stretching vibration [23].

The molybdate ion/H_2O_2 system is well known to generate ROS through the formation of peroxomolybdate intermediates [24,25]. Radical trapping experiments were conducted to identify the active species responsible for Ag dissolution (Figure 2c). Furfuryl alcohol and isopropanol were used as scavengers for $^1O_2$ and •OH, respectively. The results demonstrated that both $^1O_2$ and •OH are key active species in the leaching process, with $^1O_2$ playing a dominant role. Electron spin resonance (ESR) spectroscopy with DMPO and TEMP as spin traps was employed to further confirm the generation of ROS (Figure 2d–f). The characteristic 1:1:1 triplet signal of TEMP-$^1O_2$, the 1:2:2:1 quartet signal of DMPO-•OH, and the characteristic sextet signal of DMPO-•OOH were all observed [26–28]. The signal intensities

increased with reaction time, indicating that ROS generation begins immediately upon mixing and accumulates progressively. The DMPO-•OOH adduct is formed from the reaction between $^1O_2$ and H_2O_2.

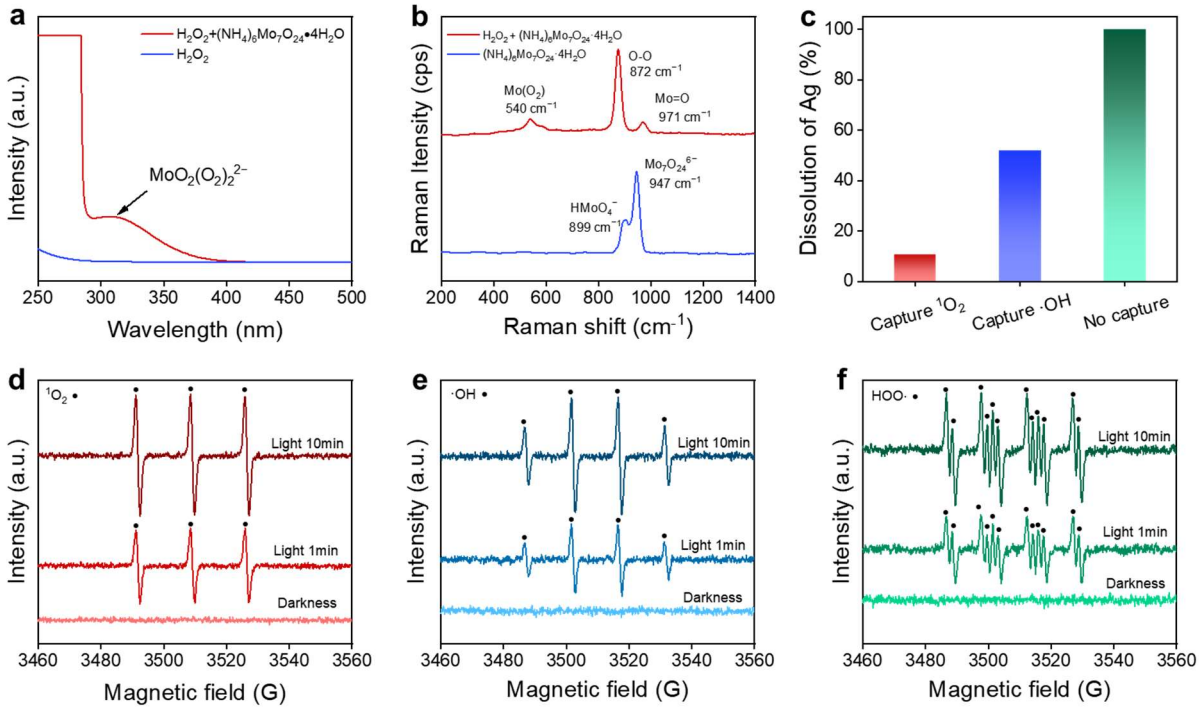


Figure 2. Mechanistic analysis of silver leaching in the $(NH_4)_6Mo_7O_{24}·4H_2O$–H_2O_2 system. (**a**) UV-vis spectra and (**b**) Raman spectra of the leaching solution. (**c**) Radical trapping experiments using furfuryl alcohol and isopropanol as scavengers for $^1O_2$ and •OH, respectively. (**d**–**f**) ESR spectra of spin adducts formed with TEMP and DMPO: (**d**) TEMP-$^1O_2$, (**e**) DMPO-•OH, and (**f**) DMPO-•OOH.

Subsequently, the recovered product obtained after silver leaching was systematically characterized to determine its morphology, composition, and chemical state. The SEM image shows that the product consists of sheet-like structures with a size of approximately 3–5 μm (Figure S5a). These sheets stack layer by layer and are uniformly distributed. The EDS mapping confirms that Ag, Mo, and O are homogeneously distributed across the product surface (Figure S5b). XPS analysis was performed to investigate the surface elemental composition and chemical bonding states [29]. The high-resolution Ag 3*d* spectrum shows two peaks at 373.9 eV and 367.9 eV, which correspond to Ag $3d_{3/2}$ and Ag $3d_{5/2}$, respectively (Figure 3a). These binding energies indicate that silver is present in the +1 oxidation state, confirming that silver was oxidized during the leaching process. The Mo 3*d* spectrum exhibits peaks at 235.4 eV and 232.4 eV, which are assigned to Mo $3d_{3/2}$ and Mo $3d_{5/2}$, respectively (Figure 3b). This indicates that Mo exists in the +6 oxidation state. The O 1*s* spectrum shows a peak at 530.4 eV, which is attributed to the molybdate ion (Figure 3a,c). The XPS survey spectrum reveals that the product contains Ag, Mo, O, a small amount of C, and a certain amount of N (Figure 3d). No Pb signal was detected in the survey spectrum. This indicates that the Pb leached during the process was not incorporated into the solid product and remained in the leaching solution, thereby enabling the separation of lead during the recovery process. The C signal likely originates from air or the sample substrate. The N 1*s* spectrum shows peaks at 398.1 eV and 401.2 eV, which correspond to N–H bonds (Figure S6).

Fourier transform infrared (FTIR) spectra were collected in the range of 400–4000 cm^{-1} to further examine the surface functional groups (Figure 3e). The bands at 3175 and 3450 cm^{-1} are assigned to the O–H stretching vibration of water molecules, and the N-ak at 1380 cm^{-1} is attributed to the bending vibration of adsorbed water [30]. The bands at 830 and 991 cm^{-1} are assigned to the O–Mo–O stretching

vibration. These results indicate that the product contains a certain amount of adsorbed water and ammonium ions. X-ray diffraction (XRD) analysis was used to determine the crystalline structure of the product (Figure 3f) [31]. The XRD peaks basically match with several standard cards of silver molybdate. The product can be identified as a mixture of multiple silver molybdate complexes with the general formula $Ag_xMo_yO_z$.

Based on these results, a reaction mechanism for Ag leaching in the $(NH_4)_6Mo_7O_{24}{\cdot}4H_2O$-$H_2O_2$ system is proposed. The molybdate ion first reacts with H_2O_2 to form the peroxo intermediate $MoO_2(O_2)_2^{2-}$ (Equation (1)). This intermediate can oxidize metallic silver through two pathways: direct oxygen transfer from the peroxo ligand to Ag^0 (Equation (2)), and generation of ROS ($^1O_2$, •OH, •OOH) that subsequently oxidize Ag^0 to Ag^+ (Equations (3) and (4)). The generated Ag^+ then reacts with molybdate ion in solution to form the silver molybdate product (Equation (5)). The specific equations are as follows:

$$MoO_4^{2-} + 2H_2O_2 \rightarrow MoO_2(O_2)_2^{2-} + 2H_2O \quad (1)$$

$$MoO_2(O_2)_2^{2-} + 4Ag + 4H^+ \rightarrow 4Ag^+ + MoO_4^{2-} + 2H_2O \quad (2)$$

$$MoO_2(O_2)_2^{2-} \rightarrow MoO_4^{2-} + 1O_2 \quad (3)$$

$$1O_2 + 2H_2O_2 \rightarrow 2 \bullet OH + 2 \bullet OOH \quad (4)$$

$$2Ag^+ + MoO_4^{2-} \rightarrow Ag_xMo_yO_z \quad (5)$$

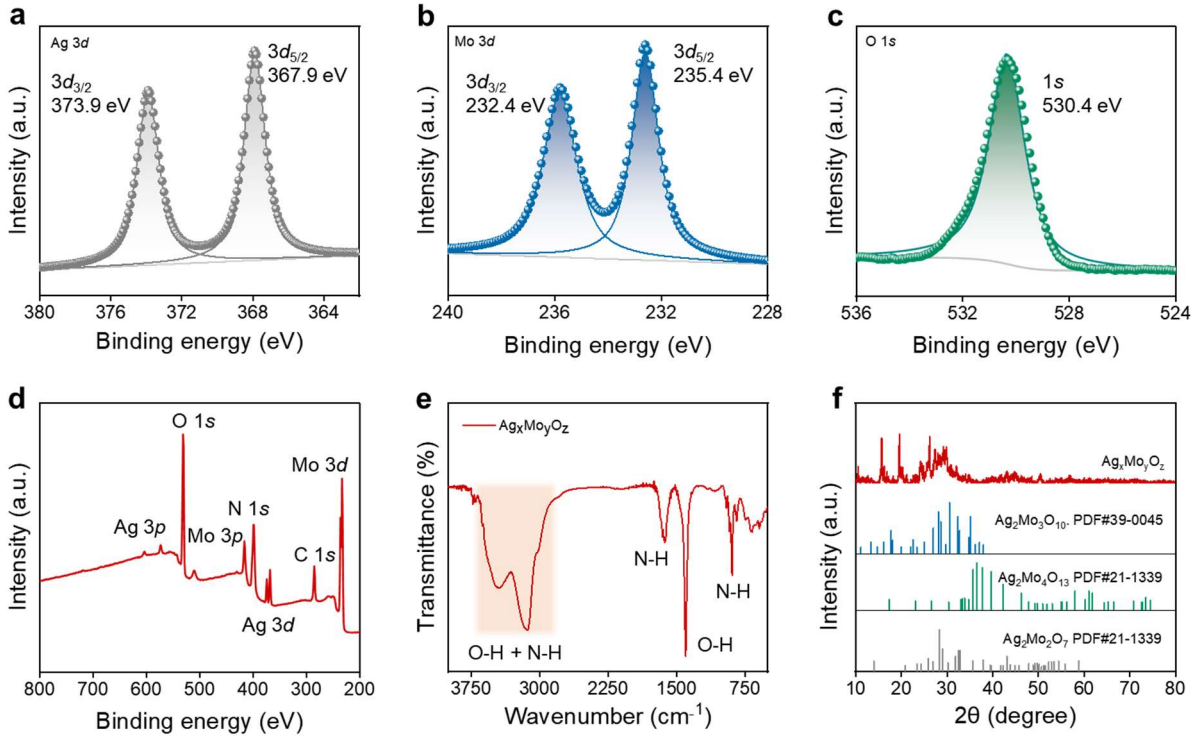


Figure 3. Characterization of the recovered product. (**a**) High-resolution Ag 3*d* XPS spectrum. (**b**) High-resolution Mo 3*d* XPS spectrum. (**c**) High-resolution O 1*s* XPS spectrum. (**d**) XPS survey spectrum. (**e**) FTIR spectrum. (**f**) XRD pattern.

3.3. Photocatalytic Degradation of Organic Pollutants by the Recovered $Ag_xMo_yO_z$

The recovered $Ag_xMo_yO_z$ was evaluated as a photocatalyst for pollutant degradation. The optical absorption properties were first examined by UV-vis spectroscopy (Figure 4a). The absorption edge of $Ag_xMo_yO_z$ is located at approximately 450 nm, indicating significant absorption in the visible light region.

The optical band gap was calculated using the Tauc equation and estimated to be about 2.64 eV (Figure 4b). The ultraviolet photoelectron spectrometer (UPS) result gives a valence band (VB) maximum of 1.8 eV (Figure S7a). Therefore, the conduction band (CB) minimum is calculated to be −0.84 eV (Figure S7b). This relatively narrow band gap suggests that $Ag_xMo_yO_z$ can be excited by visible light and has potential for photocatalytic applications [32].

Photocatalytic degradation experiments were carried out using 20 mL of 10 ppm methylene blue (MB) and rhodamine B (RhB) solutions with 50 mg of $Ag_xMo_yO_z$ catalyst under visible light irradiation for 120 min (Figure 4c–f). The results show that $Ag_xMo_yO_z$ exhibits good photocatalytic activity for both pollutants. The adsorption capacity for MB was higher than that for RhB. To distinguish between the adsorption capacity and photocatalytic performance of $Ag_xMo_yO_z$, we conducted dark adsorption experiments of MB (20 ppm) and RhB (20 ppm) on $Ag_xMo_yO_z$. The results show that MB exhibited significant dark adsorption on $Ag_xMo_yO_z$. After 120 min, C/C_0 decreased to 0.06 (Figure S8a). In contrast, RhB showed weak dark adsorption. After 120 min, C/C_0 decreased only to 0.32 (Figure S8b). This indicates that RhB removal is not mainly attributable to adsorption, whereas adsorption contributes significantly to MB removal. After the dark adsorption reached equilibrium, light irradiation was applied directly for another 120 min. The results show that MB continued to degrade under light irradiation. During the light stage, C/C_0 decreased from 0.06 to 0.02 (Figure S8a). For RhB, C/C_0 decreased from 0.32 to 0.04 during the light stage (Figure S8b). Since dark adsorption had already reached equilibrium, the further decrease in concentration under light irradiation cannot be attributed to adsorption alone. These results indicate that the recovered $Ag_xMo_yO_z$ can effectively degrade different organic dyes. The better performance for MB may be related to its molecular structure and stronger interaction with the catalyst surface. We have tested the stability of $Ag_xMo_yO_z$ by recycling the catalyst for 10 consecutive runs (Figure S9). This demonstrates the feasibility of converting retired photovoltaic panels into functional photocatalysts. The concept of treating waste with waste is validated. Further optimization of the catalyst and reaction conditions could improve the degradation efficiency and extend the application to other pollutants.

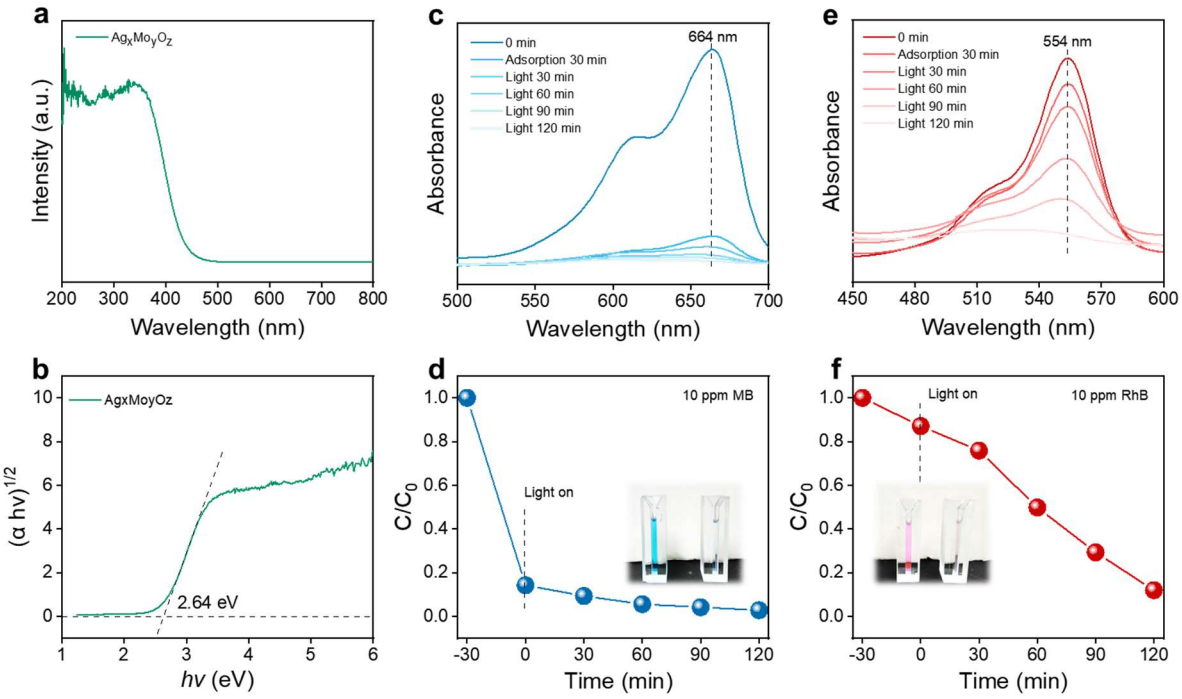


Figure 4. Photocatalytic performance of the recovered $Ag_xMo_yO_z$. (**a**) UV-vis diffuse reflectance spectrum of $Ag_xMo_yO_z$. (**b**) Tauc plot for band gap determination of $Ag_xMo_yO_z$. (**c**–**f**) Photocatalytic degradation of MB and RhB under visible light irradiation using $Ag_xMo_yO_z$.

4. Conclusions

In this work, a sustainable strategy was developed for silver recovery from end-of-life photovoltaic panels and photocatalytic valorization of the recovered product. An ammonium molybdate-H_2O_2 system selectively leached silver while aluminum remained essentially undissolved. Lead was partially leached and separated during recovery of the silver product. During leaching, Ag^+ reacted in situ with molybdate ions to form silver molybdate. The leaching process was driven by $^1O_2$, •OH, and •OOH radicals. The recovered $Ag_xMo_yO_z$ was directly used as a photocatalyst without additional purification or synthesis. It exhibited visible-light absorption with a band gap of about 2.64 eV and degraded MB completely and RhB at 90% within 120 min. These results demonstrate a closed-loop concept of treating waste with waste, converting retired photovoltaic panels into functional photocatalysts for pollutant degradation. This approach offers a promising route for sustainable management of end-of-life photovoltaic waste and simultaneous environmental remediation.

Supplementary Materials

The following supporting information can be found at: https://www.sciepublish.com/article/pii/1325, Figure S1: Effect of reagent addition mode on Ag leaching; Figure S2: Effect of different molybdenum and ammonium sources on Ag leaching; Figure S3: SEM image and corresponding EDS mapping of the back side of the PV panel, showing mainly Al and Si; Figure S4: XPS spectra of the PV panel before and after leaching: (a) Ag 3*d*, (b) Al 2*p*, (c) Pb 4*f*, and (d) Si 2*p*; Figure S5: (a) SEM image and (b) EDS mapping of the recovered product; Figure S6: High-resolution N 1*s* XPS spectrum of the recovered product; Figure S7: (a) UPS spectrum of the recovered $Ag_xMo_yO_z$. (b) Schematic energy band diagram of $Ag_xMo_yO_z$; Figure S8: Adsorption performance and photocatalytic degradation of (a) MB and (b) RhB using $Ag_xMo_yO_z$; Figure S9: Cycling stability of the recovered $Ag_xMo_yO_z$ for photocatalytic degradation of RhB under visible-light irradiation.

Acknowledgments

The authors thank Chinese Education Ministry Key Laboratory and International Joint Laboratory on Resource Chemistry, Shanghai Eastern Scholar Program, the "111 Innovation and Talent Recruitment Base on Photochemical and Energy Materials" (No. D18020), Yunnan University Collaborative Innovation Center (Qujing Green Photovoltaic Industry Collaborative Innovation Center), Technology Talent and Platform Plan Project of Yunnan Provincial Department of Science and Technology (202305AF150088), Shanghai Engineering Research Center of Green Energy Chemical Engineering (18DZ2254200), and Shanghai Frontiers Science Center of Biomimetic Catalysis.

Author Contributions

Conceptualization, X.W. (Xinru Wang) and Y.C.; Methodology, X.W. (Xinru Wang); Validation, Y.Z., X.W. (Xinwei Wang) and Z.W.; Formal Analysis, X.W. (Xinru Wang) and Y.C.; Investigation, Y.C.; Resources, Z.B.; Data Curation, X.W. (Xinru Wang) and Y.C.; Writing—Original Draft Preparation, Y.C.; Writing—Review & Editing, H.Y. (Hisao Yoshida) and H.Y. (Hiromi Yamashita); Supervision, Z.B.

Ethics Statement

Not applicable.

Informed Consent Statement

Not applicable.

Data Availability Statement

Data is available upon request.

Funding

This work was supported by the National Science Foundation of China (22525606, 22236005, 22406131, 22506126), the Innovation Program of Shanghai Municipal Education Commission (2023ZKZD50), Shanghai Leading Talent Program of Eastern Talent Plan (LJ2023002), Shanghai Government (23520711100), the Chenguang Program of Shanghai Education Development Foundation and Shanghai Municipal Education Commission (24CGA49).

Declaration of Competing Interest

The authors declare that they have no known competing financial interests or personal relationships that could have appeared to influence the work reported in this paper.

References

1. Xu W, Huang Z, Xiong X, Yang J, Zhang J, Ruan J, et al. Progress and environmental impact assessment of recycling end-of-life crystalline silicon photovoltaic modules: A comprehensive review. *J. Environ. Chem. Eng.* **2026**, *14*, 121870. DOI:10.1016/j.jece.2026.121870
2. Li F, Shaw S, Libby C, Preciado N, Bicer B, Tamizhmani G. A review of toxicity assessment procedures of solar photovoltaic modules. *Waste Manag.* **2024**, *174*, 646–665. DOI:10.1016/j.wasman.2023.12.034
3. Preet S, Smith ST. A comprehensive review on the recycling technology of silicon based photovoltaic solar panels: Challenges and future outlook. *J. Clean. Prod.* **2024**, *448*, 141661. DOI:10.1016/j.jclepro.2024.141661
4. Celep O, Deveci H, Yazici EY. A comprehensive review on recycling end of life solar photovoltaic panels. *Waste Manag.* **2025**, *206*, 115092. DOI:10.1016/j.wasman.2025.115092
5. Rout S, Jana P, Borra CR, Önal MAR. Unlocking silver from end-of-life photovoltaic panels: A concise review. *Renew. Sustain. Energy Rev.* **2025**, *210*, 115205. DOI:10.1016/j.rser.2024.115205
6. Li J, Li Y, Yu F, Hu Z, Gao Q, Li P, et al. Co-recovery of Ag and Si from PV cell panels: Directional solidification assisted by PV glass. *Sep. Purif. Technol.* **2025**, *353*, 128428. DOI:10.1016/j.seppur.2024.128428
7. Deng R, Zhuo Y, Shen Y. Recent progress in silicon photovoltaic module recycling processes. *Resour. Conserv. Recycl.* **2022**, *187*, 106612. DOI:10.1016/j.resconrec.2022.106612
8. Balaji Jadhav N, Gajare O, Zele S, Gogate N, Joshi A. Current status and challenges in silver recovery from End-of-Life crystalline silicon solar photovoltaic panels. *Sol. Energy* **2024**, *283*, 113027. DOI:10.1016/j.solener.2024.113027
9. Click N, Teknetzi I, Adcock R, Tao M, Ebin B. Silver cementation mechanism for leaching silicon solar cells in nitric acid. *Sol. Energy* **2024**, *283*, 113009. DOI:10.1016/j.solener.2024.113009
10. Chung J, Seo B, Lee J, Kim JY. Comparative analysis of I_2-KI and HNO_3 leaching in a life cycle perspective: Towards sustainable recycling of end-of-life c-Si PV panel. *J. Hazard. Mater.* **2021**, *404*, 123989. DOI:10.1016/j.jhazmat.2020.123989
11. Chen Y, Hu T, Wang X, Wang X, Wang Z, Zhang L, et al. Highly Selective Recovery of Silver from End-of-Life Photovoltaic Panels. *Trans. Tianjin Univ.* **2025**, *31*, 452–462. DOI:10.1007/s12209-025-00453-1
12. Huang Z, Guo F, Xu Z, Duan Y, Lan X, Jiang X. A recyclable solvent for recovering silver in Polysilicon photovoltaics panels: BeCl-EG-$CuCl_2$ solvents system. *J. Hazard. Mater.* **2025**, *491*, 137909. DOI:10.1016/j.jhazmat.2025.137909
13. Zhang C, Jiang J, Ma E, Zhang L, Bai J, Wang J, et al. Recovery of silver from crystal silicon solar panels in Self-Synthesized choline Chloride-Urea solvents system. *Waste Manag.* **2022**, *150*, 280–289. DOI:10.1016/j.wasman.2022.07.003
14. Chen Y, Xu M, Wen J, Wan Y, Zhao Q, Cao X, et al. Selective recovery of precious metals through photocatalysis. *Nat. Sustain.* **2021**, *4*, 618–626. DOI:10.1038/s41893-021-00697-4
15. Shang H, Chen Y, Guan S, Wang Y, Cao J, Wang X, et al. Scalable and selective gold recovery from end-of-life electronics. *Nat. Chem. Eng.* **2024**, *1*, 170–179. DOI:10.1038/s44286-023-00026-w
16. Chen Y, Guan S, Ge H, Chen X, Xu Z, Yue Y, et al. Photocatalytic Dissolution of Precious Metals by TiO_2 through Photogenerated Free Radicals. *Angew. Chem. Int. Ed.* **2022**, *61*, e202213640. DOI:10.1002/anie.202213640

17. Wahman M, Surowiak A, Forsberg K, Ebin B, Berent K, Szymczak P. Preserving silicon (Si) purity through efficient aluminum (Al) and silver (Ag) extraction and recovery from solar cell waste. *Sol. Energy Mater. Sol. Cells* **2025**, *287*, 113601. DOI:10.1016/j.solmat.2025.113601
18. Kamperidis T, Tremouli A, Remoundaki E, Lyberatos G. Silver Recovery from Wastewater, Simulating the Chemical Extract Originating from a PV Panel Using Microbial Fuel Cell Technology. *Waste Biomass Valor.* **2022**, *13*, 4073–4083. DOI:10.1007/s12649-022-01793-y
19. Qi Z, Wang S, Gao D, Bao G, Wu Z. A novel ion exchange method for recover silver and aluminum from waste crystalline silicon photovoltaic modules. *Sol. Energy* **2025**, *286*, 113142. DOI:10.1016/j.solener.2024.113142
20. Sun Y, Wang H, Cui C, Yang C, Wang Z, Ma S. Improvement of etching ability of lead-free glass frits by compositing low content PbO nanoparticles and its effect on metallization contact of solar cells. *Mater. Chem. Phys.* **2023**, *297*, 127372. DOI:10.1016/j.matchemphys.2023.127372
21. Tian SH, Tu YT, Chen DS, Chen X, Xiong Y. Degradation of Acid Orange II at neutral pH using $Fe_2(MoO_4)_3$ as a heterogeneous Fenton-like catalyst. *Chem. Eng. J.* **2011**, *169*, 31–37. DOI:10.1016/j.cej.2011.02.045
22. Arab M, Bougeard D, Aubry JM, Marko J, Paul JF, Payen E. Structure and Raman spectra of transient species in the catalytic disproportionation of hydrogen peroxide by molybdate ions. *J. Raman Spectrosc.* **2002**, *33*, 390–396. DOI:10.1002/jrs.846
23. Xia X, Guan W, Zhang G, Zhou Q, Li Q, Cao Z, et al. Formation and Stability of Molybdenum and Tungsten Species in Peroxy Solution. *J. Solution Chem.* **2023**, *52*, 551–569. DOI:10.1007/s10953-023-01249-4
24. Lin JM, Liu M. Singlet oxygen generated from the decomposition of peroxymonocarbonate and its observation with chemiluminescence method. *Spectrochim. Acta A Mol. Biomol. Spectrosc.* **2009**, *72*, 126–132. DOI:10.1016/j.saa.2008.08.019
25. Shi HC, Chen G, Wang XY, Zhang ZG. Epoxidation of α, β-unsaturated acids catalyzed by tungstate(VI) or molybdate (VI) in H_2O: Influence of pH on epoxidation rate and a quantum chemical explanation. *J. Mol. Catal. A Chem.* **2004**, *216*, 29–34. DOI:10.1016/j.molcata.2004.02.023
26. Chen S, Li Z, Wu L, Liu L, Hu J, Hou H, et al. Generation of high-valent iron-oxo porphyrin cation radicals on hemin loaded carbon nanotubes for efficient degradation of sulfathiazole. *J. Hazard. Mater.* **2023**, *444*, 130402. DOI:10.1016/j.jhazmat.2022.130402
27. Chen L, Duan J, Du P, Sun W, Lai B, Liu W. Accurate identification of radicals by in-situ electron paramagnetic resonance in ultraviolet-based homogenous advanced oxidation processes. *Water Res.* **2022**, *221*, 118747. DOI:10.1016/j.watres.2022.118747
28. Chen Y, Xu S, Fang Wen C, Zhang H, Zhang T, Lv F, et al. Unravelling the Role of Free Radicals in Photocatalysis. *Chem. Eur. J.* **2024**, *30*, e202400001. DOI:10.1002/chem.202400001
29. Xie Y, Dai Y, Yuan X, Jiang L, Zhou L, Wu Z, et al. Insight on the plasmonic Z-scheme mechanism underlying the highly efficient photocatalytic activity of silver molybdate/silver vanadate composite in rhodamine B degradation. *J. Colloid Interface Sci.* **2018**, *530*, 493–504. DOI:10.1016/j.jcis.2018.04.031
30. do Nascimento Silva Leandro MK, Barbosa Moura JV, Justino de Araújo AC, Freitas PR, Roque Paulo CL, De Sousa AK, et al. Retracted: Silver Trimolybdate ($Ag_2Mo_3O_{10}\cdot 2H_2O$) Nanorods: Synthesis, Characterization, and Photo-Induced Antibacterial Activity under Visible-Light Irradiation. *Bioinorg. Chem. Appl.* **2024**, *2024*, 1–1. DOI:10.1155/2024/9769648
31. Feng M, Zhang M, Song JM, Li XG, Yu SH. Ultralong Silver Trimolybdate Nanowires: Synthesis, Phase Transformation, Stability, and Their Photocatalytic, Optical, and Electrical Properties. *ACS Nano* **2011**, *5*, 6726–6735. DOI:10.1021/nn202296h
32. Chen Y, Deng X, Wen J, Zhu J, Bian Z. Piezo-promoted the generation of reactive oxygen species and the photodegradation of organic pollutants. *Appl. Catal. B Environ.* **2019**, *258*, 118024. DOI:10.1016/j.apcatb.2019.118024